Interfacial charge dynamics of triboelectrically-induced non-contact polypropylene/polyvinylidene fluoride sensor with low permittivity supporting layer

Petr Slobodian[1,2], Pavel Riha[2,3], Berenika Hausnerova[1,3*], Robert Olejnik[1], Jiri Matyas[1]

[1]Centre of Polymer Systems, University Institute, Tomas Bata University, Trida T. Bati 5678, 76001 Zlin, Czech Republic

[2]Department of Physics and Materials Engineering, Tomas Bata University in Zlin, Vavreckova 5669, 760 01, Zlin, Czech Republic

[3]Department of Production Engineering, Faculty of Technology, Tomas Bata University in Zlin, Vavreckova 5669, 760 01 Zlin, Czech Republic

*Corresponding author: hausnerova@utb.cz

Abstract

This work presents a simple and low-cost triboelectric sensing approach based on commercially available polypropylene (PP) films paired with polyvinylidene fluoride (PVDF) to form a triboelectric nanogenerator operating in a predominantly non-contact regime. Changes in the separation between the triboelectric layers produced measurable electrical signals without requiring sustained mechanical contact. Introducing low-permittivity polyvinyl chloride (PVC), biaxially oriented polyethylene terephthalate (BOPET), or low-density polyethylene (LDPE) sublayers under the tribonegative PVDF membrane significantly increased the induced voltage, with LDPE providing the strongest enhancement. This confirms that the dielectric permittivity of the supporting layer is a key parameter controlling the electrical output of the PP/PVDF triboelectric system. Post-contact and post-separation activation measurements showed that the PP/PVDF interface maintains triboelectrically generated charge under open-circuit conditions, and releases it only upon circuit closure, providing insight into interfacial charge dynamics relevant for non-contact operation. The sensing principle was validated under several mechanical excitations, including impulsive loading, vibration and ultrasonic stimulation, demonstrating the potential of the PP/PVDF platform for low-cost motion monitoring and self-powered signal generation.

Keywords: triboelectric nanogenerator; non-contact sensing; dielectric permittivity; motion detection; energy harvesting; packaging polymers

1. Introduction

The search for alternative sources of renewable energy in emerging technologies and the need to solve the problems of managing waste plastic packaging materials are current issues. One possible way to solve these issues is to use plastic waste for self-powered sensors. In this context, electrification between two waste plastics due to the triboelectric effect offers an effective solution for energy harvesting, as well as the self-powering. Recently, we reported that biaxially oriented polyethylene terephthalate (BOPET) films used worldwide as food packaging materials combine unique dual electrification properties that enable effective conversion of mechanical energy into electricity in a coupled piezo-triboelectric nanogenerator [1].

The triboelectric electricity generated by mechanical energy and harvested by triboelectric nanogenerators (TENGs) or used for self-powering sensors [2] is mostly investigated from the point of view of the triboelectric material pairs used, their dielectric constants, polarizability, electron affinity, ability to generate sufficient current density, and surface charge density [3]. Polarization can be increased by choosing a highly polarized dielectric, such as fluorinated polymers with negatively and positively polarized fluorine and hydrogen atoms, respectively, which enable the formation of dipoles with various configurations [3,4]. An increase in dielectric performance can also be achieved by incorporating nanoparticles into the polymer matrix of the dielectric to moderate the orientation of the dipoles [5], or by using electrospinning to produce porous dielectric fibrous structures with polymer chains that have modified dipole orientation configurations, increased contact area, higher polarization, and dielectric constants [1,3,4,6].

Polyvinylidene fluoride (PVDF) is often used in TENGs owing to its efficient electromechanical conversion. Moreover, by using PVDF copolymers or PVDF composite materials, the structure of the tribolayer of PVDF can be adjusted to increase TENGs' performance. The physical properties of PVDF can be controlled by rapid or slow cooling during PVDF film fabrication [7]. A possible increase in the triboelectric performance of PVDF involves incorporating liquid metals, such as Galinstan nanodroplets, into electrospun PVDF-co-hexafluoropropylene (PVDF-HFP) nanofibers [8]. Significantly high values of peak open-circuit voltage and power density of the TENG, reaching 1680 V and 24 W/m^2, respectively, were discussed in connection with other improved properties such as surface potential, capacitance, and charge trapping capability. The presence of liquid metal particles contributed to the secondary polarization of the PVDF-HFP, further enhancing its performance. An even higher output power density of 56 W/m^2 was achieved using a PVDF copolymer with poly(diethylene glycol methyl

ether methacrylate) combined with tribo-negative polydimethylsiloxane as the second active TENG layer [9]. The synthesis of the PVDF copolymer resulted in the transformation of the tribo-negative pristine PVDF into a tribo-positive PVDF copolymer. Another approach is to apply commonly available commercial materials, apart from the use of complex synthesized materials.

The goal of constructing a TENG is to utilize available, durable, and cost-effective commercial fabrics. This is exemplified by their use as triboelectric pairs with one fabric made of silk and the other made of polyester [10]. While this arrangement provides excellent flexibility, it results in low electromechanical conversion. However, the triboelectric output was significantly increased by more than ~17 times by adding a tribo-negative PVDF film coating to polyethylene terephthalate (PET), along with electrospun nylon 66 nanofibers on silk, thus moderating the tribo-positive performance of silk. The triboelectric short-circuit current density increased to 24.5 mA/m^2 from 1.6 mA/m^2 compared with the original silk/PET pair.

It should be also highlighted that PVDF possesses inherent piezoelectric properties [11,12]. When combined with another material, the triboelectric properties of PVDF can be studied in the course of piezo-tribo hybrid nanogenerators (PTENG) [1,13-15]. Among other materials, such as PTFE as the second part of a triboelectric pair [13], BOPET [1], or polydimethylsiloxane [15], can be mentioned. The joint piezo-tribo electrification of PVDF can be measured by a separate experiment, sequentially [12], or with a suitable experimental arrangement simultaneously [13]. It was possible to clearly distinguish between the piezoelectric and triboelectric responses of PVDF during the contact and separation phases of the TENG. Additionally, the authors enhanced the conversion efficiency of the PVDF film by incorporating ZnO nanoparticles. The piezo-tribo hybrid nanogenerator coupled with PTFE achieved a maximum output power 2.5 times higher than that of pure PVDF, reaching a value of 24.5 $\mu W/cm^2$. ZnO nanoparticles have also been applied in PTENG based on PVDF/ZnO-PDMS/rGO nanocomposites [14]. Another example is the use of an inorganic filler in PVDF piezo-tribo hybrid energy harvesting PVDF-$AlFeO_3$ composites [16] with rhombohedral or orthorhombic $AlFeO_3$ filler structures.

Recent studies demonstrate that a wide range of post-consumer plastics can be repurposed for triboelectric energy harvesting, providing a low-cost and sustainable alternative to conventional fluoropolymers. Unsorted plastic packaging waste consisting of polyethylenes (PE), polypropylene (PP), polystyrene (PS) and PET has been shown to generate substantial triboelectric, piezoelectric and pyroelectric outputs, with heterogeneous blends often outperforming single polymers due to interfacial interactions between immiscible phases [17].

Waste plastic bags and other thin-film packaging materials can also act as effective triboelectric layers, enabling simple contact–separation TENGs that deliver tens to hundreds of volts for low-power applications [18,19]. Immiscible mixtures of post-consumer thermoplastics have further been shown to enhance electricity generation in PVDF-based harvesters, where phase separation and interfacial polarization significantly increase the electromechanical response [20]. Additional approaches use recycled polymer laminates or waste-derived PET- and PS-based structures to construct tribo- or piezo-tribo hybrid nanogenerators with performance comparable to virgin materials [21]. Single-polymer waste films such as biaxially oriented polypropylene (BOPP) from packaging sources have also been identified as efficient mechano-electric transducers suitable for energy harvesting [22]. Moreover, recycled PET, PP, polyvinyl chloride (PVC) and high-density PE (HDPE) waste streams have been shown to form triboelectric pairs whose polarity ordering and dielectric contrast determine the achievable voltage output in sustainable TENG assemblies [23]. Collectively, these studies confirm that post-consumer plastics represent a technically viable and widely available resource for constructing TENG devices, supporting their use in low-cost energy harvesting and self-powered sensing applications [19].

In this study, we develop a triboelectrically-induced non-contact sensor for a motion monitoring that can simultaneously harvest electric energy from motion using paired triboelectric polymers. The basic triboelectric pair consists of two polymer nonwoven fabrics, an elecrospun PVDF layer used as a tribonegative layer, and a spun-bond PP layer used as the tribopositive layer on the Cu electrodes of the motion sensor. The triboelectric performance was further enhanced by adding a substrate layer made from waste polymer films such as PVC, BOPET, and low-density PE (LDPE). The higher electric potential due to the substrate layer increased the polarization of the PVDF layer, which significantly contributed to more efficient charge generation and an overall improvement in the measured induced voltage by the motion sensor.

2. Experimental

2.1. Materials

The dielectric PVDF polymer was purchased from Arkema (Kynar Flex® 2801, Zhejiang, China). PVDF nonwoven fiber networks were prepared by electrospinning a dimethylformamide solution. PVDF nanofibers were collected during processing on spun-bond nonwoven dielectric

polypropylene (PP). Detailed processing conditions and further details regarding the PVDF fibers and PVDF non-woven network can be found in our previous papers [1,12]. Spun-bond nonwoven PP membranes with of an area weight of 30 g/m^2 and thickness 0.3 mm were purchased from Pegatex S, PFNon-wovens s.r.o., Znojmo, Czech Republic. The PP membranes were used not only as a collecting substrate during the electrospinning process of the PVDF networks, but also as a triboelectric layer itself. The measured thickness and calculated porosity of the PP membrane were 300±30 μm and 0.82±0.02, respectively. The porosity of the PVDF membrane was 0.88±0.01. Apparent densities of PVDF and PP membranes were 0.32 ± 0.04 g/cm^3 and 0.12 ± 0.01 g/cm^3, respectively. The mass density of PVDF was (according to the supplier) 1.78 g/cm^3, and the PP mass density of compression molded film from PP membrane at 170 °C was 0.92 g/cm^3.

Three types of dielectric polymeric films made of low-density polyethylene (LDPE), biaxially oriented polyethylene terephthalate (BOPET), and polyvinyl chloride (PVC), used as food packaging plastics, were purchased from Fatra a.s., Napajedla, Czech Republic. Films with a thickness of 150 μm were used as the low-permittivity layers underlying the PVDF networks in the dielectric-to-dielectric NCM-TS.

The structures of the nonwoven PVDF and PP fiber membranes were analyzed by scanning electron microscopy (SEM; NOVA NanoSEM 450, FEI Co., Hillsboro, OR, USA). Dielectric thermal analysis (DETA) was performed using a broadband dielectric/impedance analyzer (Novocontrol Technologies GmbH & Co. KG, Montabaur, Germany). The samples were placed between two gold-plated electrodes with a diameter of 20 mm, and the relative permittivity and dielectric loss were measured in the frequency spectrum from 1 Hz to 1 MHz at room temperature.

2.2. Contact electrification measurements

A schematic of triboelectric nanogenerator (TENG) setup is shown in Fig. 1. This represents the vertical contact-separation mode to measure electrification by the PVDF/PP triboelectric pair. It consisted of two PMMA plates with dimensions of 60×60 mm and 3 mm thickness, with four metal guides equipped with springs to move the PMMA plates against each other until possible contact. The initial distance between PMMA plates was 6 mm. The PMMA plates were further equipped with Cu electrodes made of adhesive conductive Cu tape. The PP spun-bond membrane was attached to one electrode by sticking to the adhesive side of the Cu electrode made of an electrically conductive layer, and the PVDF electrospun membrane was

similarly attached to the other electrode. Measurements were performed under two types of experimental conditions, differing in the maximum pressure and approach velocity. The maximum value of the applied pressure at contact were 30 kPa and 270 kPa and the approach velocities 0.05 m/s and 0.85 m/s.

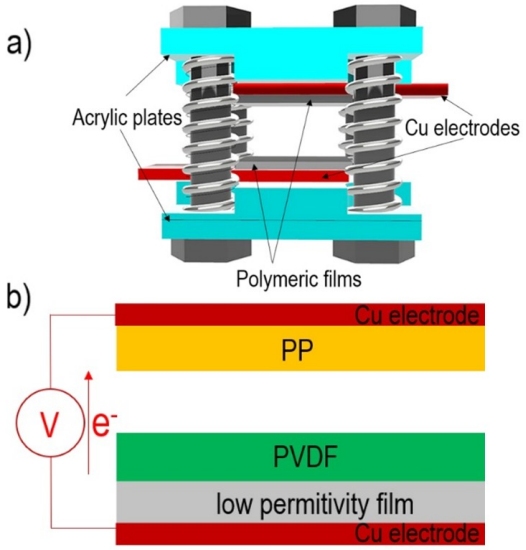

Fig. 1 a) Schematic illustration of TENG for triboelectric contact/separation measurement, b) TENG's contact triboelectric PP layer and PVDF layer on the low permittivity substrate.

The generated triboelectric output voltage was measured using an oscilloscope with an input impedance of 10 MΩ (Infinivision 1000 x-series, 4ch, 100 MHz, DSOX1204A, Keysight, Santa Rosa, CA, USA). In all the experiments, the anode was connected to a PVDF layer, which is the most negative of all the polymers used in terms of the triboelectric series. The short-circuit current density I [μAcm^{-2}] was calculated according to Ohm's law when the TENGs were connected to an electrical resistive load (22 kΩ), and the assigned voltage was measured again by an oscilloscope connected in parallel to the load. Finally, the generated charge density Q [μCm^{-2}] was measured using an electroscope-charge sensor GRG-BTA connected to a LabQuest interface system (Vernier, Edufor s.r.o., Prague, Czech Republic). The TENG was equipped with a strain gauge L6D-C3-40 kg (Zemic Europe B.V., Etten-Leur, The Netherlands) to measure the force applied in contact with the plates. An analog converter TZA11410 (VTS Zlin s.r.o., Zlin, Czech Republic) was used to power it with a ± 20mA output and 24V DC supply.

2.3. Non-contact measurements

The schematic illustrations in Fig. 2 show the non-contact mode triboelectric motion sensor and the associated energy harvester. The setup consisted of two PMMA plates with dimensions of 60×60 mm and 3 mm thickness with attached PP and PVDF tribo-layers with a BOPET substrate below PVDF.

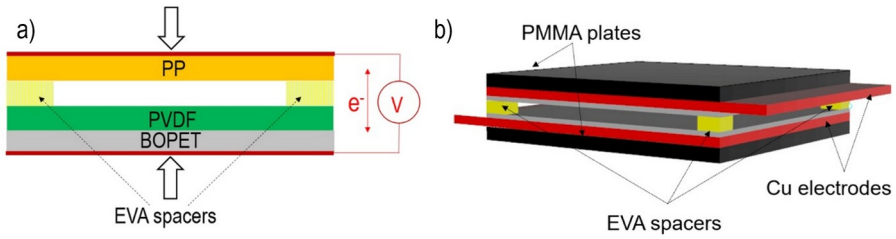

Fig. 2 Schematic of a) cross-sectional view of the PP/PVDF/BOPET stack supported by EVA spacers, b) a 3D perspective of device assembly including PMMA plates and Cu electrodes.

The gap between the plates was set using spacers made of ethylene vinyl acetate (EVA) copolymer flexible foam. When the plates were pressed against each other, the spacers controlled the reduction in the gap between the triboelectric layers and acted as springs, returning the plates to the initial space gap. Four EVA copolymer spacers with a thickness of 3 mm and a contact area of 5 mm × 5 mm were placed in the corners of the PMMA plates. During compression, the triboelectric layers approach each other, while the EVA spacers maintain a finite air gap under normal operating conditions. The sensor operates in a non-contact mode, with the induced voltage arising from electrostatic induction driven by triboelectric charges generated during the initial contact electrification step. The sensor was tested to measure the induced voltage using the PP/PVDF triboelectric pair with a BOPET substrate due to the impact of a free-fall ball from a height of 50 cm (a glass ball with a diameter of 34 mm and a weight of 52 g), amplitude of the vibration generated by placing the sensor underneath a running rotary vacuum pump, micron amplitudes of the ultrasound vibration produced by the sonication horn, and the amplitudes of cyclic stepping on the sensor. When the plates were pressed against each other, the spacers controlled the gap setting between the triboelectric layers and acted as springs, returning the plates to the initial 3 mm gap. The induced voltage generated by the sensor was used not only to determine the displacement of the detected motion, but also as a source of electric energy that could be harvested. For this purpose, a Graetz bridge rectifier equipped with four Schottky diodes (diode opening voltage 1.5 V) was used, which converted the generated triboelectric AC voltage into a DC voltage usable for low-power applications.

3. Results

Triboelectrification of the nonwoven PVDF and PP membranes is shown in Fig. 3 as a time dependence of induced triboelectric voltage in four consecutive contact/separation cycles of TENG at different approach velocities and maximum contact pressures of 0.05 m/s at 30 kPa and 0.85 m/s at 270 kPa. The voltage was induced when the electrodes with triboelectric PP and PVDF surfaces were moved against each other, touching, and separating. Cyclic-induced voltage peaks were repeatable, including negative voltage peaks appearing after PP and PVDF surface separation. The faster approach and contact pressure of the PP and PVDF triboelectric surfaces increased the generated induced voltage from about 10 V at 0.05 m/s and 30 kPa to 85 V at 0.85 m/s and 270 kPa. The voltage induction, when the triboelectric surfaces are in contact, is typically ten times higher than when they are separated. The duration of the voltage pulse reached approximately 10 ms for the contact phase, and a significantly longer time (about 40 ms) during separation.

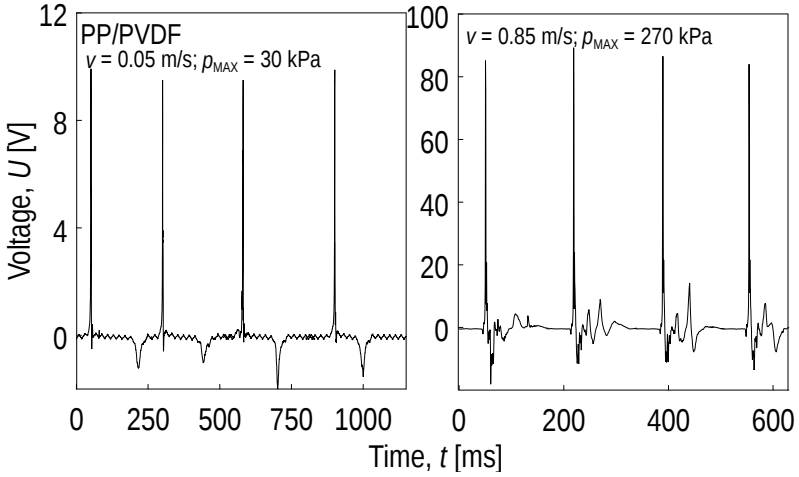

Fig. 3 Voltage induced by PVDF/PP TENG in four contact/separation cycles.

The PVDF membrane had a homogeneous structure consisting of individual fibers of submicron size with fiber diameters ranging from 0.05 to 0.3 μm. The membrane thickness was 55±5 μm. The PP nonwoven membranes were composed of straight and smooth fibers with a narrow distribution of fiber diameters of 23±3 μm. The PP membrane serves a substrate for electrospun PVDF as shown in Fig. 4. To compare the voltage induction in the porous PP and PVDF membranes with the voltage induction of their nonporous variants, the triboelectric voltage induction between the PP and PVDF films (compression molded at 190°C to 0.5 mm) was also measured. As expected, the PP and PVDF films revealed

significantly lower voltage values of 3 V and 27 V for comparable approach velocities and maximum contact pressures, i.e. 0.05 m/s at 30 kPa and 0.85 m/s at 270 kPa, respectively.

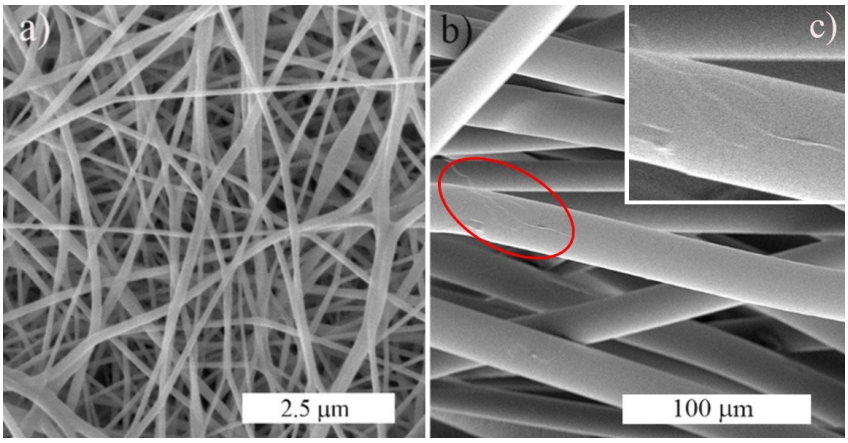

Fig. 4 SEM of a) electrospun PVDF membrane, b) spun-bond PP membrane as a substrate for PVDF with detail of PVDF fibre attached to PP membrane surface.

Underlying the triboelectric PVDF membrane with PVC, BOPET, or LDPE sublayers with a low permittivity offered the possibility to increase the performance of the nanogenerator by increasing the intensity of the electric field generated by the electric charge transfer between the PP and PVDF surfaces as shown in Fig. 5.

Fig. 5 Induced voltage by TENG in four contact/separation cycles for PVDF/PP triboelectric pair with PVC, BOPET or LDPE sublayer underneath the PVDF contacting membrane at indicated approach velocities and contact pressures.

At the approach velocity of 0.05 m/s and contact pressure of 30 kPa the induced triboelectric voltage increased to 34 V for PVC, 114 V for BOPET, and 280 V for LDPE films placed under PVDF membrane. The increase in the induced voltage for the approach velocity of 0.85 m/s and contact pressure of 270 kPa was even more pronounced reaching 335 V, 424 V, and 623 V for PVC, BOPET, or LDPE sublayers, respectively.

To relate the measured electrical outputs to the intrinsic triboelectric behavior of the tested polymers, a reference triboelectric series was constructed using a single-dielectric contact electrification test, in which each polymer was repeatedly contacted with a copper (Cu) electrode. Copper was used as a stable and well-defined tribopositive reference material.

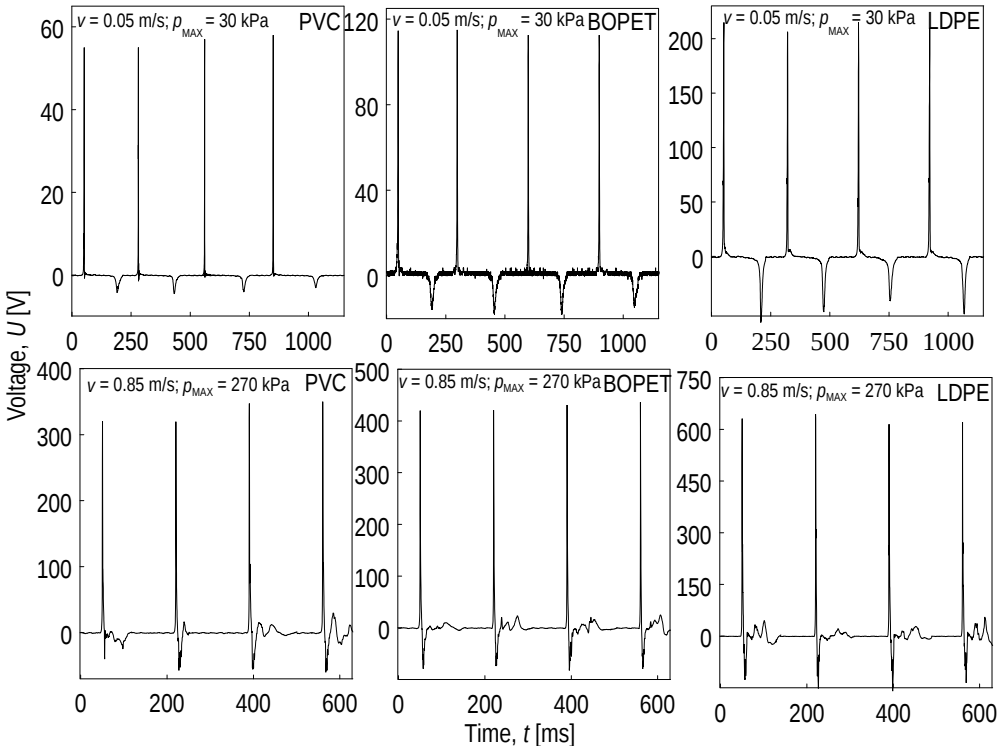

All examined packaging polymers exhibited negative charge transfer relative to Cu, allowing their mutual ordering according to the magnitude of the triboelectric charge density. The resulting sequence (Fig. 6) provides a comparative scale of tribonegativity and supports the

interpretation of the voltage and charge outputs summarized in Table 1.

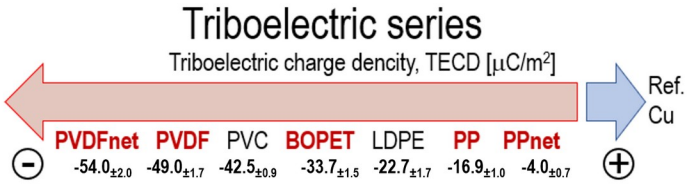

Fig. 6 Quantified triboelectric series of PVDF, PP, and the packaging polymers LDPE, BOPET, and PVC, obtained from measurements of the triboelectric charge density relative to a copper reference.

Table 1 Peak voltages U_{max}, short-circuit current density I and charge density Q of TENGs

	0.85 m/s & 270 kPa		
Triboelectric pair	U_{max} [V]	I [μAcm^{-2}]	Q [Cm^{-2}]
PP/PVDF (films)	27±3	0.7±0.1	4.1±0.3
PP/PVDF (membranes)	86±2	6.5±0.7	22.2±1.4
PP/PVDF+PVC	335±13	15.7±1.9	63.0±2.6
PP/PVDF+BOPET	424±18	24.3±2.5	71.6±2.7
PP/PVDF+LDPE	623±21	29.2±5.5	83.9±3.1

Dielectric thermal analysis was used to obtain the relative permittivity of the PVDF and PP membranes and films and PVC, BOPET, and LDPE films. The results are presented in Fig. 7 as frequency-dependent permittivity values. The relative permittivity at low frequency of 1 Hz was 13.91 (PVDF film), 6.85 (PVDF membrane), 2.11 (PP film), 5.08 (PP membrane), 3.14 (PVC film), 2.95 (BOPET film) and 2.16 (LDPE film) clearly showing the role of sublayers in the triboelectric contact/separation process. The equivalent relative permittivity of PVDF and PP comprising the triboelectric bilayer can be calculated as [1,7]:

$$\varepsilon_{r,eg} = \varepsilon_{r,PVDF} \frac{\varepsilon_{r,SUB}(d_{PVDF}+d_{SUB})}{d_{PVDF}\varepsilon_{r,PP}+d_{SUB}\varepsilon_{r,PVDF}} \quad (1)$$

where $\varepsilon_{r,PVDF}$ and $\varepsilon_{r,SUB}$ are the relative permittivities of the PVDF membrane (6.85) and a membrane sublayer (LDPE 2.16, BOPET 2.95, PVC 3.14), respectively, and d_{PVDF} and d_{SUB} are the thicknesses of the PVDF membrane (55 μm) and a sublayer (LDPE 150 μm, BOPET 150 μm; PVC 150 μm),

respectively. The reduction in the relative equivalent permittivity of the overall negative triboelectric bilayer PVDF membrane with a membrane sublayer to 4.33 for PVDF+LDPE, 5.05 for PVDF+BOPET, and 5.2 for PVDF+PVC enhanced the induced peak voltage almost four times with the PVC sublayer, five times with the BOPET sublayer, and more than seven times with the LDPE sublayer.

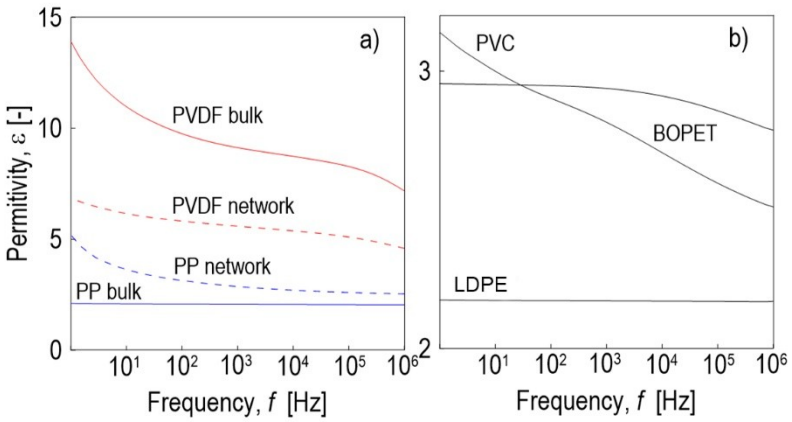

Fig. 7 Dielectric relative permittivity of a) PP and PVDF triboelectric pair, and b) PVC, BOPET and LDPE sublayers as a function of frequency at room temperature.

When the triboelectric layers are separated by an air gap during the triboelectric non-contact/separation process, their surfaces become electrically charged owing to electrostatic induction during the relative movement of the layers [24]. Testing of the PP/PVDF+BOPET triboelectric pair with the BOPET sublayer confirmed this, with the induced voltage in the TENG according to Fig. 1 increasing exponentially with increasing displacement of the PP layer towards the tribonegative PVDF layer. The displacement was set using spacers made of calibrated steel plates, placed outside the triboelectric polymer layers, stepwise from 0.6 to 1.3, 2.1, 2.4, 2.7, and 2.9 mm. The corresponding average values of ten measurements of the peak voltage induced by the TENG were 3.6, 9.1. 24.9, 34.8, 52.0, 69.9 V, Fig. 8. The relation was fitted using the exponential function $U = a[\exp(bx) - 1]$, where U is the voltage and x is the PP-layer displacement. Fitting the experimental data yielded $a = 2.52$ and $b = 1.19$ with a correlation coefficient of $R = 0.989$.

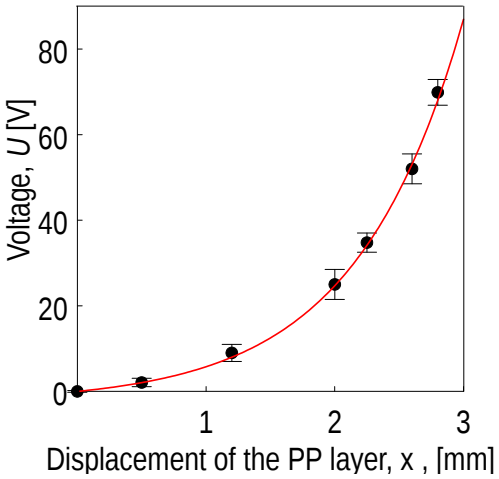

Fig. 8 Peak induced voltages as a function of the PP-layer displacement during non-contact triboelectric separation cycles.

The operating principle of the triboelectrically induced non-contact sensor relies on electrostatic induction between the already triboelectrically charged PP and PVDF surfaces: when the tribopositive PP layer is brought closer to the tribonegative PVDF layer by a compressive force, the electric field across the air gap changes, inducing a voltage that reflects the PP-layer displacement. The EVA spacers (3 mm) set the nominal separation between the triboelectric layers and maintained the air gap throughout the measurements (see Fig. 2). When the compressive force was released, the foam spacers acted as springs and restore the plates to their initial position. To test the sensor, repeated stepping on the sensor, impact of a glass ball, vibrations from a rotary vacuum pump and ultrasonic horn were used as sources to apply a compressive force, Fig. 9.

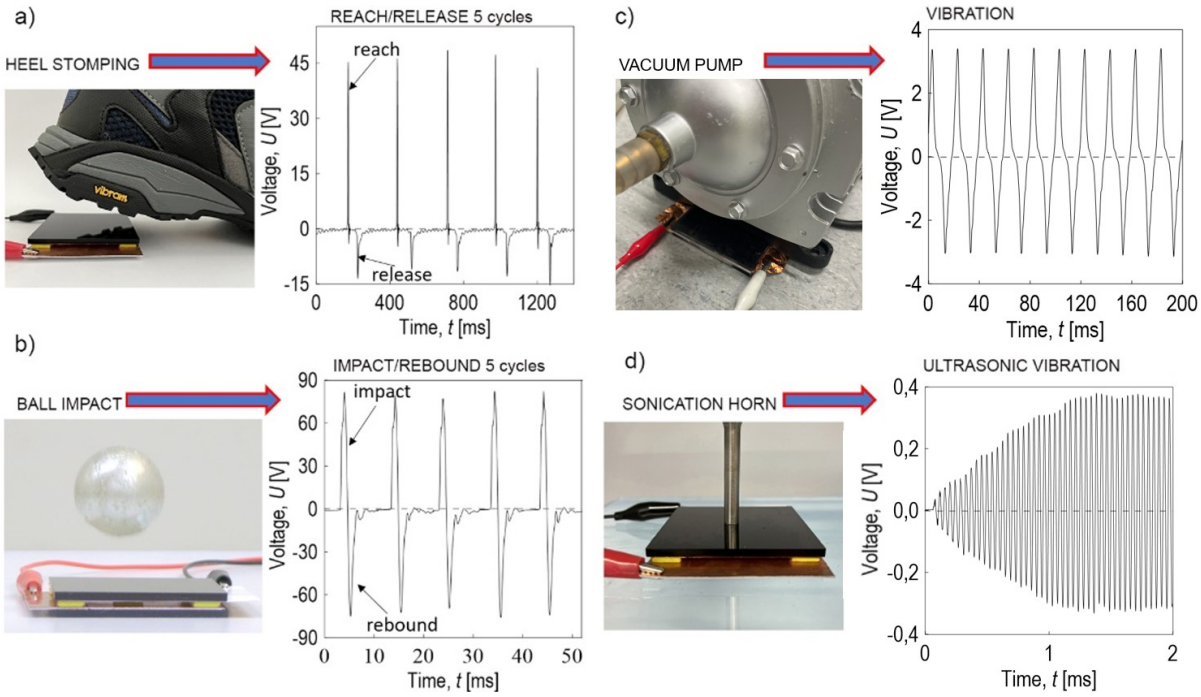

Fig. 9 Voltage responses of triboelectrically-induced non-contact sensor to different types of mechanical excitation: (a) heel stomping, (b) ball impact, (c) vibrations generated by a rotary vacuum pump, and (d) ultrasonic vibration from a sonification horn.

Simultaneously, the induced AC voltage generated by the periodic displacement of the triboelectric layers can be converted into DC electric energy by the Graetz full-bridge rectifier and used for low-consumption supplies. The data in Fig. 10 show the voltage values and the corresponding number of charge cycles, with a maximum of 300 V after 40 steps on the sensor surface. After the capacitor was charged, the circuit was short-circuited, and the course of the discharge voltage over time for different numbers of cycles was recorded using an oscilloscope. The exponential voltage drop lasted 250 ms. Another example is the lighting of eight LED diodes connected in series after 10 steps on this non-contact mode triboelectric sensor (see insert in Fig. 10).

To further examine the dielectric polarization processes contributing to the triboelectric output, additional experiments were performed in which the PP/PVDF triboelectric pair with BOPET sublayer was subjected to a controlled post-contact and post-separation electrical activation. These measurements followed the general procedure illustrated in Fig. 1, in which the triboelectric layers were either brought into direct contact or fully separated while the external circuit remained open, and the electrical response was recorded only after reconnecting the electrodes.

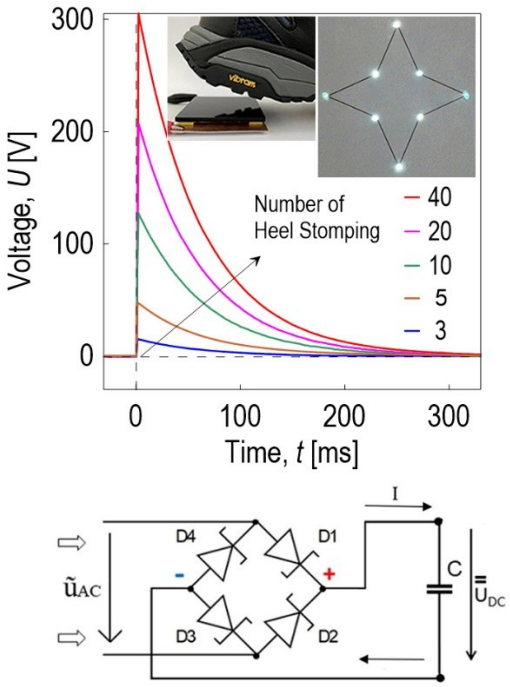

Fig. 10 The time dependence of the discharge voltage for different numbers of electrification by repeated steps on the sensor and the schematics of the Graetz full-bridge rectifier with store capacitor.

In the post-contact experiment, the PP and PVDF with BOPET sublayer were first brought into contact and kept in this state, while the external circuit remained open. Any residual charge on the Cu electrodes was removed by short-circuiting before the contact phase. The contact generated the interfacial triboelectric charge at the PP-PVDF boundary under open-circuit conditions. Approximately 0.5 s after the layers had been brought into contact, while they were still held in this fully contacted state, the switch in the external circuit was closed, initiating charge flow that produced a measurable voltage transient. The resulting time-dependent voltage response (Fig. 11) exhibited an exponential decay characteristic of a capacitor discharge, with a maximum induced voltage of approximately +40 V and a corresponding triboelectric charge density of about +12.6 μCm^{-2}. This behaviour reflects the redistribution of the stored interfacial charge once the electrodes are electrically connected. These post-contact measurements also confirm that the PP/PVDF interface retains triboelectrically generated charge under open-circuit conditions. This charge retention is essential for the operation of the sensor in its non-contact mode, where the induced voltage arises solely from electrostatic induction due to changes in the air-gap distance, without requiring repeated physical contact of the surfaces.

Complementary to the post-contact activation, the post-separation experiment was performed to demonstrate that the charge state established during contact also persists when the layers are mechanically separated under open-circuit conditions, which is essential for the non-contact operation of the sensor. In the post-separation experiment, the electrodes were first short-circuited to remove any residual charge, after which the PP and PVDF layers were separated under open-circuit conditions. During this separation, the triboelectric charge generated during the preceding contact phase could not redistribute or discharge, because the external circuit remained open. Once the layers reached the fully separated state, the switch in the external circuit was closed, triggering charge flow in the opposite direction to that observed in the post-contact case. The resulting voltage transient (Fig. 12) exhibited a negative peak with a magnitude of approximately −22 V and a corresponding triboelectric charge density of about −5.8 μCm⁻². After the initial peak, the signal decayed exponentially in the same manner as a discharging capacitor. This behavior reflects the electrical release of the interfacial charge state that remained electrically isolated during open-circuit separation and became able to redistribute only after the electrodes were connected.

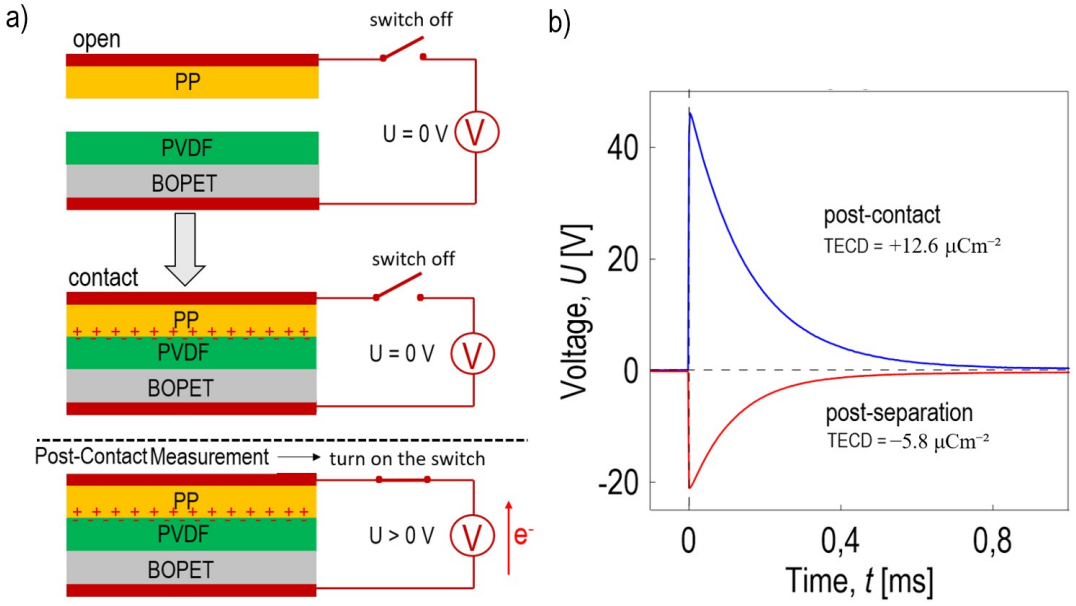

Fig. 11 a) Schematic of the post-contact and post-separation activation procedure for the PP/PVDF triboelectric pair with BOPET sublayer illustrating the open-circuit contact, open-circuit separation, and subsequent electrical activation after closing the switch, and b) corresponding voltage transients measured after the external circuit is closed.

These measurements demonstrate that the interface maintains a mechanically induced interfacial charge state under open-circuit conditions and releases it only upon the circuit closure, effectively behaving as a mechanically polarized capacitor. The ability of the interface to preserve this mechanically imposed polarization without requiring continuous physical contact is fundamental for the operation of the sensor in its non-contact mode, where the electrical output arises solely from electrostatic induction caused by changes in the air-gap distance. This behaviour not only validates the underlying non-contact sensing mechanism but also opens possibilities for delayed signal generation and passive charge storage.

4. Discussion

The behavior of the investigated PP/PVDF triboelectric pair can be interpreted by combining their relative triboelectric tendencies with the influence of dielectric permittivity on a charge induction. Measurements of the triboelectric charge density against a copper reference confirmed that all polymers used in this study are tribonegative with respect to Cu, with PVDF and its netted variant exhibiting the highest negative charge densities. PP is less tribonegative, consistent with its positive polarity in the PP/PVDF pair. This polarity ordering is reflected in the voltage outputs of the TENG structures listed in Table 1.

The effect of the dielectric environment was examined by introducing LDPE, BOPET and PVC sublayers of different permittivity under the tribonegative PVDF surface. Both earlier experimental reports and theoretical modelling [25-28] indicate that low-permittivity sublayers enhance the electric field between the triboelectric surfaces by limiting field screening within the dielectric. This enhances the electric field reaching the electrode, increases the induced charge, and therefore raises the open-circuit voltage. Our results agree with this trend: the LDPE, BOPET and PVC sublayers, all having lower permittivity than PVDF, systematically increased the induced voltage. Among the tested sublayers, LDPE provided the largest enhancement of the induced voltage, with BOPET and PVC showing progressively smaller increases, in line with their relative permittivities.

In the non-contact configuration, the electrical output was governed by the instantaneous distance between the tribopositive PP and the tribonegative PVDF surfaces. As the separation decreased, the electric field across the air gap intensified, resulting in higher induced voltage. The measured voltage-distance dependence exhibited an exponential trend within the tested range reflecting the strong sensitivity of the induction process to small changes in the air gap. This behaviour demonstrates that the PP/PVDF pair can reliably transduce relative plate motion into an electrical signal in a predominantly non-contact configuration**.** This principle was further validated by testing the system as a self-powered sensor under various model excitations, including impulsive loading, vibration and ultrasonic stimulation, where the induced voltage not only enabled motion detection but could also be harvested for low-power applications.

Additional post-contact and post-separation measurements provided insight into charge retention at the PP/PVDF interface. Charge generated during contact or separated under open-circuit conditions remained stored until the external circuit was reconnected, at which point a transient voltage corresponding to the release of this interfacial charge was observed. The opposite polarities of the post-contact and post-separation transients confirm that the direction of charge flow depends on whether the stored state was created during touching or during separating of the layers. This behaviour resembles a mechanically conditioned capacitive element in which the mechanical step defines the stored charge state while the electrical output occurs only upon circuit closure.

Additional post-contact and post-separation measurements provided deeper insight into the interfacial charge behaviour of the PP/PVDF system. The triboelectric charge generated during contact, or maintained during open-circuit separation, remained electrically isolated and therefore unable to redistribute until the external circuit was closed. Upon reconnection, a transient voltage was produced whose polarity reflected the mechanical history of the interface: a positive peak for post-contact and a negative peak for post-separation. This behaviour is characteristic of a mechanically polarized capacitor, in which a mechanical step defines the interfacial polarization state, while the electrical response is activated only when the circuit is closed. Such mechanically imposed charge states are fundamental for the predominantly non-contact sensing mode demonstrated in this work, where the induced voltage arises solely from electrostatic induction due to changes in the air-gap distance. This

decoupling of mechanical excitation from electrical activation also suggests opportunities for delayed signal generation and passive charge storage in future triboelectric sensor architectures.

5. Conclusion

A triboelectric sensing system based on the PP/PVDF pair was developed and experimentally validated for the detection of motion and low-power energy harvesting. Operating in a predominantly non-contact regime, the system converted changes in a plate separation into electrical signals without requiring sustained mechanical contact between the triboelectrically charged surfaces. Introducing polymeric sublayers with lower permittivity beneath the tribonegative PVDF surface substantially increased the induced voltage, with LDPE providing the strongest enhancement. This confirms that the dielectric permittivity of the supporting layer is a key parameter for tuning the electrical output in the system.

The sensing principle was demonstrated under a range of mechanically relevant excitations, including impulsive loading, vibration and ultrasonic stimulation, which generated self-powered voltage signals. Post-contact and post-separation activation measurements further showed that the PP/PVDF interface retains triboelectrically generated charge under open-circuit conditions and releases it upon circuit closure, providing additional insight into interfacial charge dynamics and demonstrating the versatility of the system.

Overall, the results show that the PP/PVDF platform, supported by low-permittivity sublayers and operating in a predominantly non-contact regime, provides an effective triboelectric sensing system with added energy-harvesting capability, offering a simple and low-cost route to motion monitoring and self-powered signal generation.

Acknowledgements

This publication was created as part of the implementation of the project Testing laboratory for the implementation of sustainable and resilient technologies, reg. number CZ.02.01.01/00/23_021/0010411, co-financed by the European Union under the OP Jan Amos Comenius. This work was also supported by the Ministry of Education, Youth, and Sports of the Czech Republic within the framework of DKRVO (RP/CPS/2024-28/005).

Declaration of interests

The authors have no conflicts to disclose.

Ethical Compliance

Any procedure performed in this study does not involve human participants.

Data Aviability

The datasets generated and/or analyzed during the current study are available upon request.

References

[1] P. Slobodian, R. Olejnik, J. Matyas, P. Riha, B. Hausnerova, 2023. A coupled piezo-triboelectric nanogenerator based on the electrification of biaxially oriented polyethylene terephthalate food packaging films. Nano Energy. 118, 108986. https://doi.org/10.1016/j.nanoen.2023.108986.

[2] J. Chen, C. Zhang, W. Xuan, L. Yu, S. Dong, Y. Xie, W. Yin, J. Luo, 2019. Triboelectric nanogenerator-based self-powered resonant sensor for non-destructive defect detection. Sensors. 19, 3262. https://doi.org/10.3390/s19153262.

[3] X. Wang, B. Yang, J. Liu, Y. Zhu, C. Yang, Q. He, A flexible triboelectricpiezoelectric hybrid nanogenerator based on P(VDF-TrFE) nanofibers and PDMS/ MWCNT for wearable devices, Sci. Rep. 6 (2016) 1–10. https://doi.org 10.1038/srep36409.

[4] M.M. Rastegardoost, O.A. Tafreshi, Z. Saadatnia, S. Ghaffari-Mosanenzadeh, C.B. Park, H.E. Naguib, 2023. Porous PVDF mats with significantly enhanced dielectric properties and novel dipole arrangement for high-performance triboelectric nanogenerators. Applied Materials Today. 30, 101732. https://doi.org/10.1016/j.apmt.2023.101732.

[5] J. Chen, H. Guo, X. He, G. Liu, Y. Xi, H. Shi, C. Hu, Enhancing performance of triboelectric nanogenerator by filling high dielectric nanoparticles into sponge PDMS film, ACS Appl. Mater. Interfaces 8 (2016) 736–744. https://doi.org/10.1021/ACSAMI.5B09907.

[6] P. Slobodian, R. Olejnik, J. Matyas, B. Hausnerova, P. Riha, R. Danova, D. Kimmer, 2022. Electrical detection of vibrations of electrospun PVDF membranes. Int. J. Mol. Sci. 23, 14322. https://doi.org/10.3390/ijms232214322.

[7] Y. Liu, J. Mo, Q. Fu, Y. Lu, N. Zhang, S. Wang, S. Nie, 2020. Enhancement of triboelectric charge density by chemical functionalization. Adv. Func. Mat. 30, 2004714. https://doi.org/10.1002/adfm.202004714.

[8] Z. Sha, C. Boyer, G. Li, Y. Yu, F.-M. Allioux, K.-Z. Kourosh, C.-H. Wang, J. Zhang, 2022. Electrospun liquid metal/PVDF-HFP nanofiber membranes with exceptional

triboelectric performance. Nano Energy., 92, 106713. https://doi.org/10.1016/j.nanoen.2021.106713.

[9] T. Kamilya, M. Pakhira, P. Sarkar, Md Yousuf Sk, S. Naskar, S. Acharya, Robust nanogenerators based on tribo-positive graft copolymers of tribo-negative poly(vinylidene fluoride). ACS Applied Electronic Materials. 5 (2023) 126521-6530. https://doi.org/10.1021/acsaelm.3c01005.

[10] D.G. Jeong, Y.J. Ko, D.W. Lee, Y.M. Kwak, H. Kim, K.T. Lee, M. Lee, J.H. Jung, Intriguing triboelectrification behavior of identical P(VDF-TrFE) polymers. Current Applied Physics. 29 (2021) 122-127. https://doi.org/10.1016/j.cap.2021.07.003.

[11] S. Bairagi, G. Khandelwal, X. Karagiorgis, S. Gokhool, C. Kumar, G. Min, D.M. Mulvihill, High-performance triboelectric nanogenerators based on commercial textiles: electrospun Nylon 66 nanofibers on silk and PVDF on polyester. ACS Applied Materials & Interfaces. 14 (2022) 44591-44603. https://doi.org/10.1021/acsami.2c13092.

[12] J. Li, Q. Meng, W. Li, Z. Zhang, Influence of crystalline properties on the dielectric and energy storage properties of poly(vinylidene fluoride). J. Appl. Polym. Sci. 122 (2011) 1659-1668. https://doi.org/10.1002/app.34020.

[13] H.H. Singh, N. Khare, Neeraj, Flexible ZnO-PVDF/PTFE based piezo-tribo hybrid nanogenerator. Nano Energy. 51 (2018) 216-222. https://doi.org/10.1016/j.nanoen.2018.06.055.

[14] S. Ojha, P. Maity, S. Bera, S.K. Si, B.B. Khatua, 2023. Metal–organic framework–derived ZnO-assisted β-phase-stabilized high-performance PVDF/ZnO-PDMS/rGO nanocomposites as piezo–tribo hybrid nanogenerator. Energy Technology. 11, 2300157. https://doi.org/10.1002/ente.202300157.

[15] Z. Yu, M. Chen, Y. Wang, J. Zheng, Y. Zhang, H. Zhou, D. Li, Nanoporous PVDF hollow fiber employed piezo–tribo nanogenerator for effective acoustic harvesting. ACS Applied Materials & Interfaces. 13 (2021) 26981-26988. https://doi.org/10.1021/acsami.1c04489.

[16] A. Sasmal, S. Maity, A. Arockiarajan, S. Sen, Electroactive properties and piezo-tribo hybrid energy harvesting performances of PVDF-$AlFeO_3$ composites: role of crystal symmetry and agglomeration of fillers. Dalton Transactions. 2023, 52, 41, 14837-14851. https://doi.org/10.1039/D3DT02547K.

[17] P. Slobodian, P. Riha, B. Hausnerova, Unsorted postconsumer plastic waste in energy conversion using piezoelectric, triboelectric, and pyroelectric generation mechanisms. ACS Sustainable Chemistry & Engineering. 13 (2025) 2683-2693. https://doi.org/10.1021/acssuschemeng.4c06984.

[18] X. Feng, Q. Li, K. Wang, Waste plastic triboelectric nanogenerators using recycled plastic bags for power generation. ACS Applied Materials & Interfaces. 13 (2020) 400-410. https://doi.org/10.1021/acsami.0c16489.

[19] G. Han, B. Wu, Y. Pu, A triboelectric nanogenerator based on waste plastic bags for flexible vertical interconnection system. Microsystem Technologies 26 (2020) 3893-3899. https://doi.org/10.1007/s00542-020-04879-6.

[20] P. Slobodian, B. Hausnerova, P. Riha, V. Pata, R. Olejnik, J. Matyas, 2025. Turning plastic waste immiscibility into an advantage: efficiency improvement of PVDF-based energy harvesters using post-consumer thermoplastics. Advanced Materials Interfaces. 12, 2500070. https://doi.org/10.1002/admi.202500070.

[21] N. Kumar Das, S. Badhulika, 2024. Recyclable waste derived green triboelectric nanogenerator for self-powered synthesis of defect-free graphene via mechano-electrochemical exfoliation. Chemical Engineering Journal. 480, 147897. https://doi.org/10.1016/j.cej.2023.147897.

[22] P. Slobodian, P. Riha, B. Hausnerova, 2025. Mechano-electric conversion of biaxially oriented polypropylene films from plastics-packaging waste sources. Chemical Engineering Journal. 524, 169157. https://doi.org/10.1016/j.cej.2025.169157.

[23] V.A. Jarvio-Cordova, E.A. Elvira-Hernández, A. García-Saldaña, J.D. Garay-Marín, G.E. Ovando-Chacón, M. Díaz-González, E. Delgado-Alvarado, G. Mora-Aquino, A. Herrera-May, 2025. Sustainable triboelectric nanogenerator based on recycled and waste materials for renewable energy harvesting. Renewable Energy. 251, 123439. https://doi.org/10.1016/j.renene.2025.123439.

[24] X. Fu, X. Pan, Y. Liu, J. Li, Z. Zhang, H. Liu, M. Gao, 2023. Non-contact triboelectric nanogenerator. Advanced Functional Materials 33, 2306749. https://doi.org/10.1002/adfm.202306749.

[25] G. Min, L. Manjakkal, D.M. Mulvihill, R. Dahiya, Triboelectric nanogenerator with enhanced performance via an optimized low permittivity substrate. IEEE Sensors 20 (2019) 6856-6862. https:// doi.org/10.1109/JSEN.2019.2938605.

[26] R.L. Bulathsinghala, A. Ravichandran, H. Zhao, W. Ding, R.D.I.G. Dharmasena, 2024.

The intrinsic impact of dielectric constant on output generation of triboelectric nanogenerators. Nano Energy. 123. 109383. https://doi.org/10.1016/j.nanoen.2024.109383.
[27] R.D.I.G. Dharmasena, K.D.G.I. Jayawardena, C.A. Mills, J.H.B. Deane, J.V. Anguita, R.A. Dorey, S.R.P. Silva, Triboelectric nanogenerators: providing a fundamental framework. Energy & Environmental Science, 10 (2017) 1801–1811. https://doi:10.1039/c7ee01139c.
[28] R.D.I.G. Dharmasena, K.D.G.I. Jayawardena, C.A. Mills, R.A. Dorey, S.R.P. Silva, A unified theoretical model for triboelectric nanogenerators, Nano Energy 48 (2018) 391–400. https://doi.org/10.1016/j.nanoen.2018.03.073.